REPORT
doi:10.26443/seismica.v2i4.1674

Shoreline crossing Moho geometry of the Cascadia slab: CascadiaMoho1.0

Asif Ashraf * [1], **Emilie E. E. Hooft** [1]

[1]Department of Earth Sciences, University of Oregon, USA

Author contributions: *Conceptualization*: Asif Ashraf, Emilie Hooft. *Formal Analysis*: Asif Ashraf. *Writing - Original draft*: Asif Ashraf, Emilie Hooft. *Writing - Review & Editing*: Asif Ashraf, Emilie Hooft. *Supervision*: Emilie Hooft.

Abstract Accurate characterization of subducting slab geometry is fundamental to understanding the distribution of earthquakes, the dynamics of arc volcanism, and the assessment of seismic hazards. Well-constrained slab structures also serve as critical inputs for geophysical imaging and geodynamic modeling efforts that aim to resolve key processes in subduction zones. In this study, we present a comprehensive, margin-wide model of the Moho associated with the subducting oceanic plate beneath the Cascadia subduction zone, developed through the integration of publicly available offshore and onshore datasets. We integrate high-resolution seismic reflection data from the offshore CASIE21 expedition with three previously published, lower-resolution onshore slab models (McCrory et al., 2012; Hayes et al., 2018; Bloch et al., 2023) to construct a unified Moho surface. This synthesis produces six alternative Moho geometries, enabling flexibility for studies that require varying structural assumptions. The accompanying open-source workflow offers a transparent and adaptable approach for combining heterogeneous datasets. In areas lacking direct constraints, Moho depths were estimated through interpolation from adjacent regions. The resulting models provide a valuable foundation for analyzing along-strike variations in slab structure and their implications for Cascadia geodynamics.

Production Editor:
Christie Rowe | Alice Gabriel
Handling Editor:
Brendan Crowell
Copy & Layout Editor:
Aisling O'Kane

Received:
March 28, 2025
Accepted:
December 22, 2025
Published:
February 2, 2026

Non-technical summary Understanding the shape and depth of the oceanic tectonic plate as it sinks beneath North America in the Cascadia region is important because it helps explain where earthquakes happen, how volcanoes are fed, and how to better assess seismic risks. Here, we present a detailed and unified view of the crust–mantle boundary (known as the Moho) that is driving the the oceanic plate beneath the Cascadia region. To create this view, we combined highly detailed offshore seismic images from a recent marine expedition with previously published onshore models. By merging these datasets, we produced six different versions of the Moho that other researchers can choose from based on the needs of their own studies. Our method offers a simple, flexible and open-source workflow to combine different types of data, and scientists can adjust the settings to create a version that fits their specific study. In some areas where no data exists, we estimated the Moho location using nearby information. The result is a set of comprehensive models that describe how the structure of the subducting slab varies along the Cascadia margin.

1 Introduction

Developing a margin-wide oceanic slab structure advances our understanding of subduction zone architecture and dynamics (Schellart and Rawlinson, 2010). Structural heterogeneities in the subducting slab structure can control seismicity patterns and stress accumulation (Carbotte et al., 2024; Ashraf et al., 2025; Ashraf and Filina, 2023b). In addition, a detailed description of the geometry of the subducting slab—including its depth variations, segmentation, and lateral continuity—provides critical insights into the interplay between inherited lithospheric features and ongoing tectonic processes (Carbotte et al., 2024; Baes et al., 2011; Magni et al., 2017; Biemiller et al., 2024). These observations allow scientists to refine geophysical and geodynamic models by offering robust constraints that capture the complexities of subduction mechanics, thereby improving seismic hazard assessments (Kincaid, 1995; Gerya and Meilick, 2011).

This report presents shoreline-crossing Moho geometries associated with the subducting oceanic crust along the Cascadia Subduction Zone (CSZ) (Fig. 1). The CSZ is a ~1000 km convergent margin from Northern California to Vancouver Island, capable of generating megathrust earthquakes that pose a significant risk of seismic hazard in the Pacific Northwest (Wang and Tréhu, 2016). Furthermore, Cascadia's unique characteristics–including a young, warm subducting plate (Gao et al., 2017) and unusually low levels of present-day seismicity (Acharya, 1992)–make it an important natural laboratory for tectonic and geophysical research (Toomey et al., 2014). A detailed model of the subducting slab plays a vital role in this research as it illuminates the architecture of the subducting and overriding plates thereby giving us insights into their mechanical behaviors. A robust, margin-wide slab model thus offers critical constraints for geodynamic models of subduction

*Corresponding author: aashraf@uoregon.edu

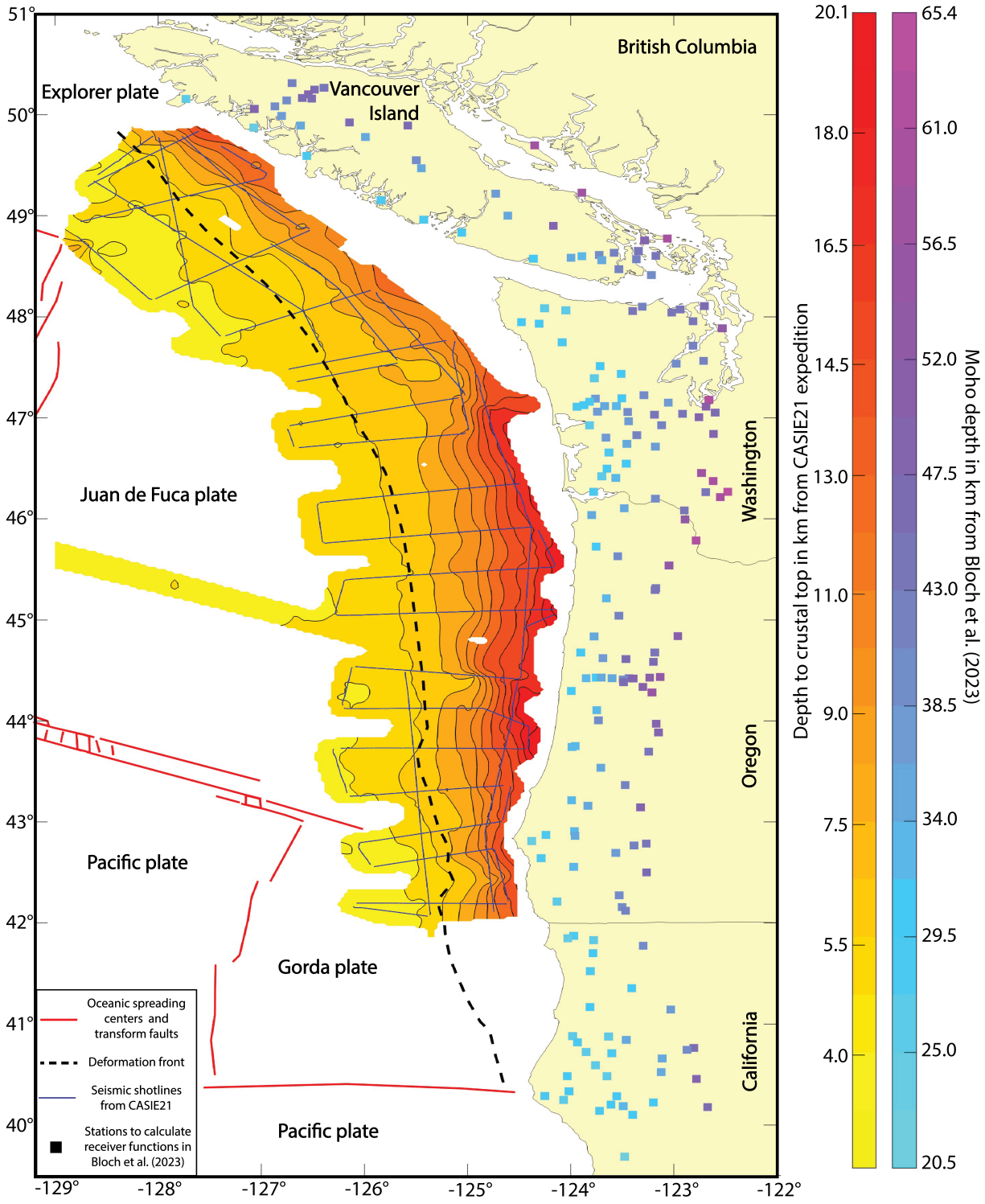

Figure 1 Map of the CSZ illustrating the geometry of the subducting slab from two complementary datasets. Offshore, the crustal topography is from the CASIE21 expedition (Carbotte et al., 2024) and is depicted with color-filled contours at 1.5 km intervals, where contour boundaries are indicated by black lines. Onshore, Moho depths from Bloch et al. (2023) are represented as colored squares marking the locations of seismic stations for which receiver function analyses were performed. See Section 2 for additional details on these datasets.

and other geophysical studies, improving seismic hazard assessment (Yepes et al., 2016; Laurencin et al., 2018; Parsons et al., 1998).

However, a high-resolution, margin-wide slab structure in the CSZ that integrates shoreline-crossing data is currently absent from the literature. Existing margin-wide onshore slab models (Bloch et al., 2023; Hayes et al., 2018; McCrory et al., 2012) exhibit high uncertainty (mostly around 2-4 km) in the nearshore region (Ashraf et al., 2025), a crucial area for evaluating future megathrust slip behavior. Moreover, the newly acquired CASIE21 seismic reflection data, collected offshore from northern Vancouver Island, Canada, to southern Oregon, USA, provide unprecedented reso-

lution of the basement (Carbotte et al., 2024). A coherent slab model that effectively bridges this high-resolution offshore data with lower-resolution onshore data is missing from the literature.

To address the persistent gap in nearshore constraints and to provide consistent starting models for geophysical and geological investigations, we present a systematic integration of high-resolution offshore crustal geometry from the CASIE21 expedition with lower-resolution onshore slab models. This effort yields a coherent, margin-wide, shore-crossing Moho surface that serves as a practical proxy for the subducting slab and offers new insight into the crustal architecture of the CSZ. We generate six alternative Moho geometries by applying two distinct smoothing approaches across one offshore and three onshore datasets, ensuring broad incorporation of available published constraints. The accompanying MATLAB-based workflow is designed to be transparent, accessible, and adaptable, enabling researchers to construct customized slab geometries for diverse geophysical applications. Importantly, the workflow is straightforward to update as new datasets become publicly available, allowing for iterative refinement of the model in support of ongoing community efforts.

2 Data

We retrieve subducting slab information for CSZ that is publicly available for the published literature. The retrieved datasets can be divided into two categories: the offshore (shallower) part and an onshore (deeper) part. For the offshore portion, we incorporated depth to the top of crust (or basement) data from the Cascadia Seismic Imaging Experiment 2021 (CASIE21), which acquired 5,500 km of multi-channel seismic (MCS) reflection profiles (Fig. 1) using a 12–15 km-long receiver array (Carbotte et al., 2024). The survey spanned 900 km along the plate boundary, covering from the northern Gorda Plate to offshore Vancouver Island, with intersecting margin-crossing and parallel profiles forming a quasi-regular grid. Depth uncertainty, in this dataset, varies with location and data quality. In the outer 20 km seaward of the deformation front, where MCS data are densest and reflectors are well-imaged, slab surface depths are accurate to within 50–100 m. Within the outer accretionary wedge, uncertainty increases modestly to 100–300 m due to slightly weaker reflections and reliance on reflection tomography. Beneath the continental shelf, where reflections degrade and velocity structure becomes harder to constrain, errors grow to 300–900 m. A gap in offshore Northern California represents the only unexamined portion of the subduction margin in this dataset. The CASIE21 dataset is further complemented by MCS data collected over the Juan de Fuca (JdF) plate, spanning from the JdF Ridge to the trench offshore of Oregon (Han et al., 2016).

For the onshore, deeper part of the subducting slab, we use data from three sources. First, we incorporate Moho information from Bloch et al. (2023), who analyzed receiver functions from 298 onshore broadband seismic stations to model the crustal structure as three layers over a mantle half-space, defining the Moho of the oceanic plate as the 'm' interface. Synthetic receiver functions were generated using ray-theoretical modeling of plane-wave scattering at these interfaces, and quality measures and nominal depth uncertainties were assigned based on the consistency of back-scattered phases and the scatter of local minima in the parameter space. In this dataset, vertical errors are smallest (2-3 km) in Central Oregon. Uncertainty grows to 3-5 km beneath the Olympic Peninsula and Vancouver Island as thick sediments, shallow dip, and 3D velocity variations blur the receiver-function phases. Uncertainty in the southern Klamath/Cape Mendocino segment, imaged by a sparser network in tectonically contorted crust, reaches 5–7 km. Offshore portions that rely on artificial control points, and downdip regions where the slab signal vanishes, exceed 7–10 km because depth is effectively extrapolated rather than observed. In our analysis, we omitted the lowest-quality data—marked with an 'X' in Bloch et al. (2023)—where the characteristic slab signature is decisively absent.

The second source for the deeper subducting slab is the top-of-slab information from McCrory et al. (2012). They compiled a comprehensive database of depth control points from various seismic data sources, including earthquake hypocenters, active- and passive-source seismic velocity profiles, seismic reflection data, and resistivity profiles. To ensure reliability, they assigned different weights to these data types, giving the highest priority to earthquake locations because they directly map the slab's upper surface. They then employed two complementary approaches to construct the three-dimensional slab model. First, they manually hand-contoured the weighted control points to capture observed warps and buckles, and second, they used a computer-generated interpolation with polynomial splines via the GMT Surface tool for a smoother representation. The uncertainty in this dataset varies by region and data quality. In well-constrained areas like northern California depth uncertainty is low, around 2–3 km. In regions like Puget Sound and Vancouver Island, differing interpretations between passive and active seismic data lead to uncertainties of 4–8 km. Oregon, with sparse data and large interpolation gaps, has much higher uncertainties of 8–10 km. Offshore Oregon areas, constrained only by trench geometry and assumed sediment thickness, exceed 10 km uncertainty. These variations stem from uneven data coverage, velocity model biases, and ambiguity in mapping the true slab surface.

The third dataset of deeper subducting slab we use is the global Slab2.0 model from Hayes et al. (2018). They developed Slab2.0 by first compiling an extensive, multi-source database that includes active source seismic interpretations, receiver functions, relocated seismicity catalogs, and tomographic data. They then directly modeled the three-dimensional structure of each subduction zone by computing slab depth at individual grid nodes and interpolating these discrete measurements into a continuous surface. To integrate the diverse data types—with their varying uncertainties—they applied an oriented elliptical search filtering

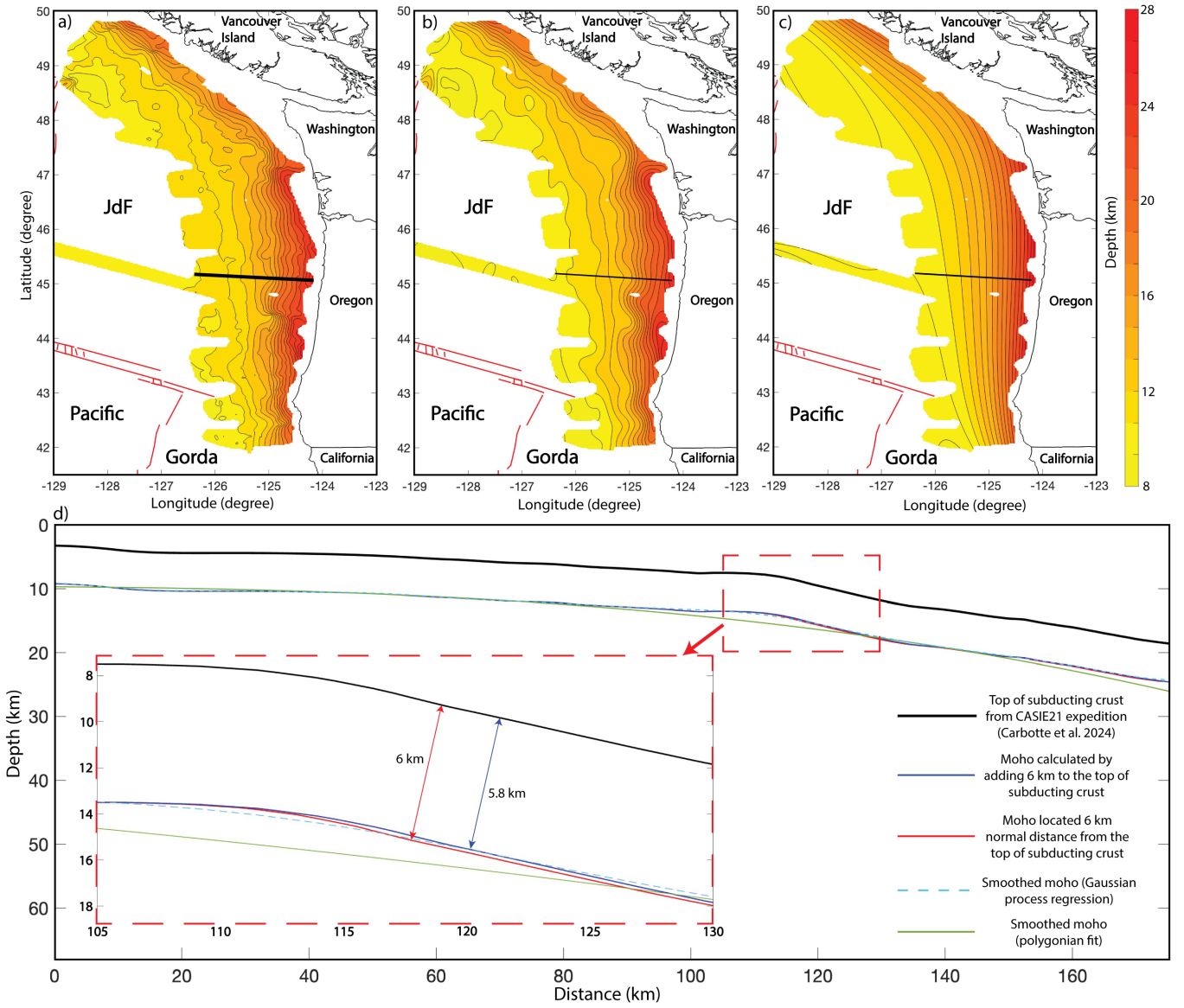

Figure 2 Moho depth estimations derived from the top of the crust data of CASIE21 expedition (Carbotte et al., 2024). (a) Moho surface defined as a 6 km depth normal to the CASIE21 basement. (b) Moho surface after Gaussian process regression, which smooths high-frequency undulations. (c) Moho surface after a fourth-order polynomial fit, further smoothing medium-to-high frequency variations. (d) Cross-section along the profile marked by the black line in (a), illustrating the CASIE21 top of the crust alongside the different Moho depth models.

at each node and combined the results into a probability density function, whose peak defines the slab center. The continuous slab surface was generated using a least squares spline interpolation and smoothed with a Gaussian filter, with special procedures implemented to accurately represent vertical or overturned slab segments.

3 Methods

3.1 Conversion of Basement to Moho depth

The primary objective of this study is to develop a comprehensive, margin-wide model of the Moho structure of the subducting oceanic crust. We compiled publicly available slab data that primarily includes measurements of the Moho depth. In some instances, however, the available data represent the top of the crust or basement, such as the CASIE21 reflection data and slab top information from McCrory et al. (2012), that needs to be converted into Moho depth. Basement depths were converted to Moho depths by assuming a 6 km average slab thickness of the oceanic slab (Carbotte et al., 2024; Ashraf and Filina, 2023b; Han et al., 2016). Two primary challenges must be addressed before converting basement data into Moho interface. The first issue is the crustal thickness constraint. Simply adding 6 km (average thickness of JdF slab) to the basement depth is not a valid approach due to the high dip angle of the subducting slab (Fig. 2). When defining the Moho as a constant-thickness offset from top of the subducting crust or basement, it is crucial to measure this offset perpendicularly (i.e., along the local normal) to the basement. Merely subtracting or adding a fixed vertical distance (e.g., 6 km) would not guarantee uniform

thickness in regions where the basement is inclined or curved. Instead, an offset measured along the local normal ensures that the resultant Moho surface maintains the specified thickness, regardless of local topographic slope. The second issue is surface roughness. The basement topography exhibits short-wavelength roughness, which must be smoothed to ensure that the Moho interface captures only long-wavelength deformation.

3.1.1 Determination of local normal vector

To implement a consistent thickness while converting basement data to Moho, we first represent the basement as a continuous function

$$z = f(x, y),$$

where x and y define the lateral coordinates of the subsurface grid and z is the depth to the basement. We then compute the surface partial derivatives

$$f_x = \frac{\partial f}{\partial x}, \quad f_y = \frac{\partial f}{\partial y}.$$

These derivatives quantify the slope in each horizontal direction. The basement surface can be equivalently defined by the implicit equation

$$F(x, y, z) = z - f(x, y) = 0.$$

By vector calculus, the gradient of F—denoted ∇F—is normal to the surface $F(x, y, z) = 0$. Evaluating ∇F yields

$$\nabla F = \big(-f_x, -f_y, 1\big),$$

which, although normal to the surface, is not necessarily of unit length. Thus, we normalize this vector to obtain the *local unit normal*:

$$\hat{\mathbf{n}}(x, y) = \frac{1}{\sqrt{1 + f_x^2 + f_y^2}} \big(-f_x, -f_y, 1\big).$$

This unit vector points in the direction perpendicular to the basement surface at each (x, y).

Once the local normal vector is determined, the Moho depth at each grid cell is found by displacing the basement coordinates $\big(x, y, f(x, y)\big)$ by the desired thickness d along $\hat{\mathbf{n}}(x, y)$. For a deeper Moho, the offset is typically applied downward, so the new depth becomes

$$z_{\text{Moho}} = f(x, y) - d\,\hat{n}_z(x, y),$$

with corresponding shifts in the x and y directions given by

$$x_{\text{Moho}} = x - d\,\hat{n}_x(x, y), \quad y_{\text{Moho}} = y - d\,\hat{n}_y(x, y).$$

This procedure guarantees a uniform orthogonal separation between basement and Moho, thereby achieving the prescribed thickness regardless of the basement's local slope or curvature.

3.1.2 Smoothing of basement roughness

In our Moho calculation, we remove the high-frequency roughness of the basement by applying two different filters with varying degrees of smoothness. First, we apply the non-parametric, probabilistic method, Gaussian process regression (similar to Kriging in geostatistics) that models the data as a realization of a Gaussian process using kernel functions to capture spatial correlations with hyperparameters optimized by maximizing the likelihood. This step removes high-frequency features while preserving medium frequencies (Fig. 2b). Second, a fourth-order polynomial regression is applied to retain only the very low-frequency component, yielding a smoothed Moho surface that reflects only the long-wavelength bending of the subducting slab (Fig. 2c). Together, these filtering approaches ensure a robust representation of the underlying geological structure across multiple spatial scales (Fig. 3).

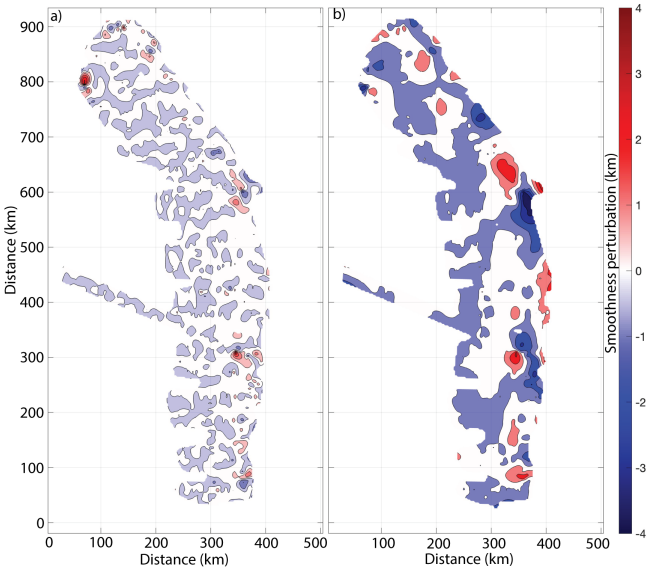

Figure 3 Maps showing differences between the CASIE21 basement-derived Moho (Fig. 2a) and its smoothed versions. 'a' shows differences resulting from smoothing with Gaussian Process Regression (Fig. 2b), while '1b' shows differences from smoothing using a polynomial fit (Fig. 2c).

3.2 Developing a margin-wide Moho

In this study, we developed comprehensive, margin-wide model of the Moho structure using high-resolution offshore data and lower-resolution onshore data from public sources that cover most of the margin. However, some regions of the CSZ lack data coverage. One such gap occurs along the offshore California segment, which was not surveyed during the CASIE21 marine expedition. To address this gap, we extend the across-strike profile derived from the southern portion of the polygonal-fit Moho model up to the southernmost extent of the subduction zone, between 40.5° and 41.5° latitude. Another significant gap in our coverage is the Moho section adjacent to and beneath the Gorda Ridge, between -128.2° and -126.2° longitude (Fig. 4). Given the minimal sedimentary cover in this area (Gardner et al.,

1993), the bathymetric data effectively represents the basement topography. We add 6 km to the bathymetric data to approximate the Moho depth and apply Gaussian smoothing to generate a refined Moho model for this region.

After addressing the significant data gap, we integrate Moho information from four sources (Fig. 4): (1) the offshore Moho derived from the CASIE21 expedition, (2) the onshore low-resolution Moho, (3) the Moho for Northern California constructed by extending the smoothed Moho structure from the southern Oregon boundary, and (4) the Moho beneath and near the Gorda Ridge based on bathymetric data. Nearest-neighbor interpolation is then applied to generate a coherent, margin-wide Moho model for the entire CSZ.

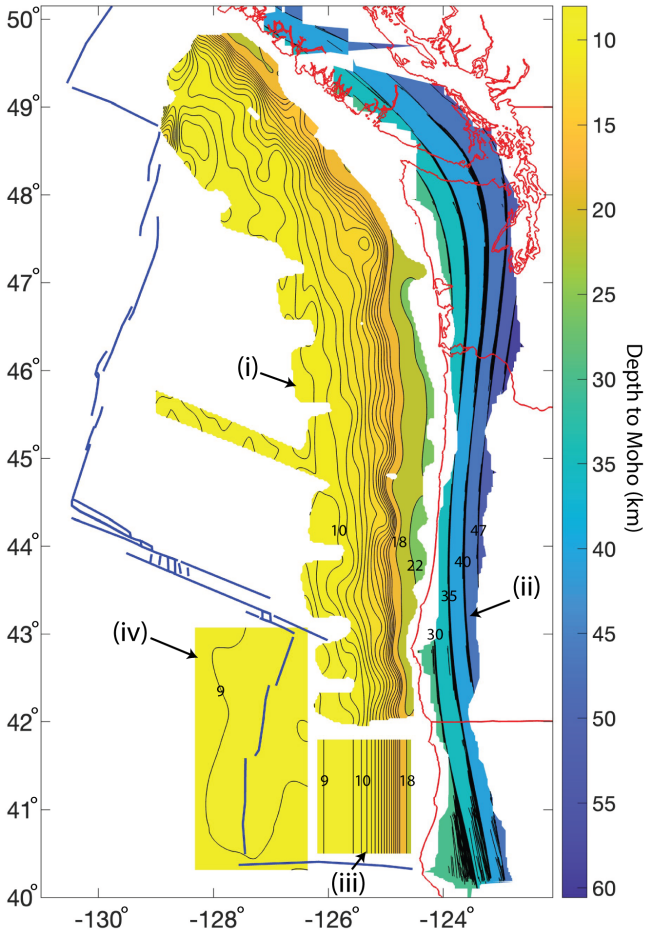

Figure 4 Compilation of the Moho data from different areas of the CSZ gathered to construct a coherent margin-wide Moho model for the oceanic slab. We gather Moho patches from four distinct data sources (i) the offshore Moho derived from the CASIE21 expedition; (ii) the onshore low-resolution Moho from Bloch et al. (2023); (iii) the 2.5D Moho for Northern California obtained by extending the smoothed Moho structure from the southern Oregon boundary; and (iv) the Moho beneath and near the Gorda Ridge inferred from bathymetric data. See Section 3.2 for more details.

4 Results and Future Directions

In this study, we present unified, margin-wide Moho geometries across the CSZ, effectively bridging previous gaps between offshore and onshore datasets. Our model addresses the Moho interface in the critical near-shoreline region, characterized by structural complexity (Gao and Long, 2022), material heterogeneity (Ashraf et al., 2025), and significant geodynamic implications (Carbotte et al., 2024) within subduction zone environments. We present this coherent, shore-crossing Moho geometry as a proxy for the subducting slab structure in CSZ. Our approach assumes a constant thickness of the oceanic crust, which is an acknowledged simplification. In reality, the oceanic crust exhibits inherited structural variability, including features such as propagator wakes (Ashraf and Filina, 2023a), causing local thickness variations of around 1 km (Marjanović et al., 2011).

The six Moho geometry models are derived from publicly available, peer-reviewed datasets detailing the depth of the subducting slab. In cases where datasets provided information only on the top of the subducting slab we estimated the Moho depth by applying a consistent 6 km offset in the normal direction from the basement surface. Conversely, datasets that explicitly included Moho depth measurements were used directly without significant modification.

Integrating datasets across the shoreline boundary presents substantial challenges due to marked differences in data resolution. The offshore region benefits from high-resolution seismic data with low uncertainty, while the onshore region depends on lower-resolution, broader-scale seismic data, resulting in higher uncertainty. Such differences can introduce discontinuities or artifacts when merging these datasets, potentially obscuring important geophysical features (Ars et al., 2024). We overcome this issue by implementing a careful data curation and preparation strategy, followed by straightforward linear interpolation techniques designed to create a coherent, continuous transition from high-resolution offshore data to comparatively lower-resolution onshore observations. This approach ensures a smooth and geologically meaningful representation of the Moho across the shoreline. Additionally, we addressed the inherent roughness of basement surfaces when converting basement depth to Moho depth, particularly evident in the CASIE21 basement reflection data and bathymetric measurements around the Gorda Ridge. For CASIE21 basement reflections, we employed two methods to reduce roughness: Gaussian regression smoothing, which effectively removed roughness at scales around 50 km, typically resulting in vertical adjustments within 1 km (occasionally reaching 2 to 3 km) (Fig. 3a); and 4th-order polynomial fitting, which significantly smoothed the Moho interface by removing roughness at scales of approximately 100 to 150 km, predominantly resulting in vertical shifts within 2 km but occasionally ranging from 3 to 4 km (Fig. 3b).

Fig. 5 illustrates the Moho geometries derived from integrating multiple publicly available datasets. The resulting six Moho models span latitudes from 40.5°N to 50°N and longitudes from 128.5°W to 122.25°W. Along-

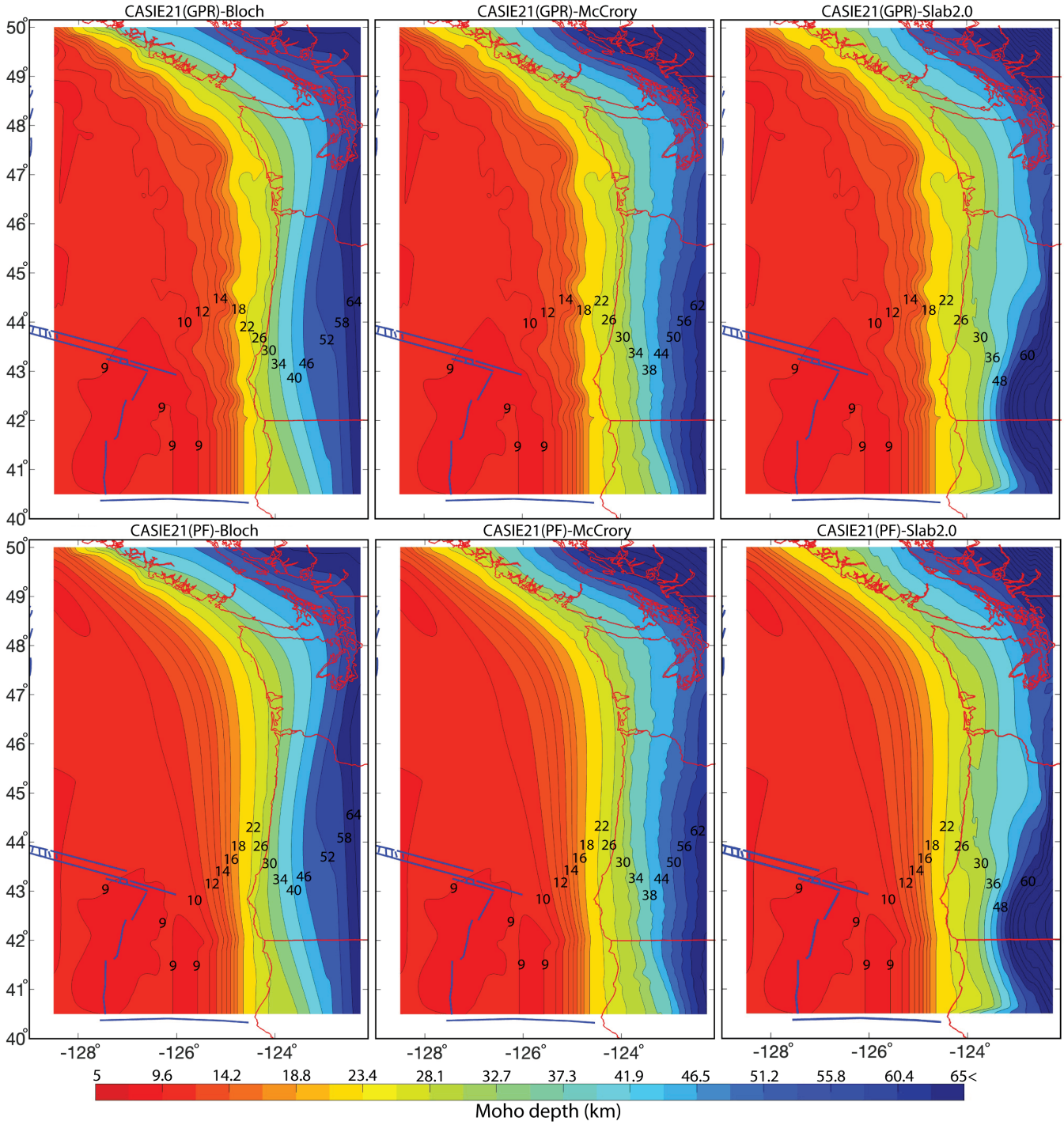

Figure 5 CascadiaMoho1.0: Six models for the shore-crossing Moho geometry across the CSZ, derived by combining offshore CASIE21 data with three onshore slab-depth datasets. In this figure, the onshore slab data are referred to as Bloch, McCrory and Slab2.0 which are respectively from Bloch et al. (2023), McCrory et al. (2012) and Hayes et al. (2018). The top panel shows the combined Moho smoothed using Gaussian process regression (GPR), and the bottom panel shows the Moho smoothed via polynomial fitting (PF). Contours are shown at intervals of 1 km from 5–16 km depth, 4 km from 16–30 km, and 6 km beyond 30 km.

strike, this region extends from just north of the Mendocino triple junction and Northern California in the south to British Columbia and the Explorer plate in the north. Across-strike coverage extends from the westernmost boundaries of the Juan de Fuca plate in offshore to about 150–200 km onshore. Four distinct dataset types were combined, and linear interpolation was performed to generate these integrated, shore-crossing Moho interfaces.

This study currently relies on slab depth information only from published onshore and offshore observations. However, these publicly available datasets, when combined, lack direct observations in several key regions. One such gap exists offshore Northern California, where no public slab depth data are available. To address this, we extrapolated an average depth profile from southern Oregon into the northern California margin. Ongoing efforts to reprocess and analyze legacy

seismic data in this region (Shuck et al., 2024) are expected to help close this data gap and provide direct observational constraints. Another approximation in this study is the assumption of a uniform 6 km thickness for the oceanic slab. Ongoing works utilizing CASIE21 reflection data aim to measure slab thickness more precisely by directly imaging the oceanic Moho (Boston et al., 2024). These results will enable future versions of the model to incorporate independently constrained Moho depths, reducing reliance on inferred slab-top information. In addition, PmP arrivals from CASIE21 offshore seismic shots recorded on Cascadia2021 onshore nodal seismometers illuminate the near-shore Moho structure (Ashraf et al., 2024). This region has previously lacked sufficient resolution in both offshore and onshore datasets. Currently, these results are only available for two limited regions in central (Nolan et al., 2022) and south-central Oregon (Ashraf et al., 2025). We anticipate that these ongoing efforts—combining new analyses of legacy data, refined slab thickness measurements, and improved imaging of the nearshore Moho—will significantly enhance the accuracy and continuity of the Moho interface in future versions of this model. These advancements will be integrated into the next iteration of the Cascadia Moho.

5 Conclusion

This study presents CascadiaMoho1.0, a unified, margin-wide shore-crossing geometry of the Moho of the oceanic crust in the CSZ that integrates high-resolution offshore seismic reflection data from the CASIE21 expedition with several lower-resolution onshore datasets from the literature. We generated six distinct Moho geometries that reconcile offshore and onshore structural variations. Through the systematic conversion of basement depths to Moho depths—using a normal-offset approach—and the application of robust smoothing techniques, the resulting models effectively bridge the gap between disparate data sources. Our interpolation method creates a smooth transition between offshore and onshore datasets, mitigating artifacts that could arise from differences in data resolution. By addressing challenges such as data resolution disparities and limited near-shore coverage, this work establishes a comprehensive framework that can serve as a foundation for future coherent and comprehensive geophysical and geodynamic model-building efforts.

Future work will focus on refining this model by incorporating additional datasets, particularly offshore Northern California from legacy seismic data, direct Moho observation from CASIE21 datasets, and the nearshore region of the margin from the PmP arrivals on the Cascadia2021 onshore nodal seismometers. These improvements will lead to an even more comprehensive and updated representation of the Cascadia slab structure. For now, the CascadiaMoho1.0 model, openly accessible to the research community, serves as a foundational resource offering essential constraints for geophysical analysis, geodynamic simulations, and seismic hazard assessments.

Acknowledgements

This research was supported by the Cascadia Region Earthquake Science Center (CRESCENT) through funding provided by a donation from the Pacific Gas and Electric Company.

Data and code availability

The source code, models, and figure plots developed in this study are publicly available at: https://zenodo.org/records/15036984.

Competing interests

The authors have no competing interests.

References

Acharya, H. Comparison of seismicity parameters in different subduction zones and its implications for the Cascadia subduction zone. *Journal of Geophysical Research: Solid Earth*, 97(B6): 8831–8842, 1992. doi: 10.1029/92JB00069.

Ars, J.-M., Tarits, P., Hautot, S., and Bellanger, M. Geophysical models integration using principal component analysis: application to unconventional geothermal exploration. *Geophysical Journal International*, 239(3):1789–1798, 2024. doi: 10.1093/gji/ggae357.

Ashraf, A. and Filina, I. New 2.75-D gravity modeling reveals the low-density nature of propagator wakes in the Juan de Fuca plate. *Tectonophysics*, 869:230127, 2023a. doi: 10.1016/j.tecto.2023.230127.

Ashraf, A. and Filina, I. Zones of Weakness Within the Juan de Fuca Plate Mapped From the Integration of Multiple Geophysical Data and Their Relation to Observed Seismicity. *Geochemistry, Geophysics, Geosystems*, 24(10):e2023GC010943, Oct. 2023b. doi: 10.1029/2023GC010943.

Ashraf, A., Hooft, E. E., and Toomey, D. R. High-resolution shore-crossing 3-D seismic tomographic model in Southern Oregon. In *AGU Fall Meeting Abstracts*, volume 2024, pages T43D–02, 2024.

Ashraf, A., Hooft, E. E. E., Toomey, D. R., Tréhu, A. M., Nolan, S., Wirth, E. A., and Ward, K. M. A High-Resolution 3-D P-Wave Velocity Structure of the South-Central Cascadia Subduction Zone From Wide-Angle Shore-Crossing Seismic Refraction Data. *Journal of Geophysical Research: Solid Earth*, 130(2): e2024JB029525, Feb. 2025. doi: 10.1029/2024JB029525.

Baes, M., Govers, R., and Wortel, R. Subduction initiation along the inherited weakness zone at the edge of a slab: Insights from numerical models. *Geophysical Journal International*, 184(3): 991–1008, 2011. doi: 10.1111/j.1365-246X.2010.04896.x.

Biemiller, J., Gabriel, A.-A., May, D., and Staisch, L. Subduction zone geometry modulates the megathrust earthquake cycle: Magnitude, recurrence, and variability. *Journal of Geophysical Research: Solid Earth*, 129(8):e2024JB029191, 2024. doi: 10.1029/2024JB029191.

Bloch, W., Bostock, M. G., and Audet, P. A Cascadia Slab Model From Receiver Functions. *Geochemistry, Geophysics, Geosystems*, 24(10):e2023GC011088, Oct. 2023. doi: 10.1029/2023GC011088.

Boston, B., Carbotte, S. M., Han, S., Shuck, B., Beeson, J. W., Canales, J. P., Nedimovic, M. R., and Tobin, H. J. Megathrust Step-down into Igneous Oceanic Crust at the Cascadia Subduc-

tion Zone and its Implications for Seismogenesis. In *AGU Fall Meeting Abstracts*, volume 2024, pages T53A–3187, 2024.

Carbotte, S. M., Boston, B., Han, S., Shuck, B., Beeson, J., Canales, J. P., Tobin, H., Miller, N., Nedimovic, M., Tréhu, A., et al. Subducting plate structure and megathrust morphology from deep seismic imaging linked to earthquake rupture segmentation at Cascadia. *Science Advances*, 10(23):eadl3198, 2024. doi: 10.1126/sciadv.adl3198.

Gao, D., Wang, K., Davis, E. E., Jiang, Y., Insua, T. L., and He, J. Thermal state of the E xplorer segment of the C ascadia subduction zone: Implications for seismic and tsunami hazards. *Geochemistry, Geophysics, Geosystems*, 18(4):1569–1579, 2017. doi: 10.1002/2017GC006838.

Gao, H. and Long, M. D. Tectonics and Geodynamics of the Cascadia Subduction Zone. *Elements*, 18(4):226–231, 08 2022. doi: 10.2138/gselements.18.4.226.

Gardner, J. V., Cacchione, D., Drake, D., Edwards, B., Field, M., Hampton, M., Karl, H. A., Kenyon, N. H., Masson, D., McCulloch, D., et al. Map showing sediment isopachs in the deep-sea basins of the Pacific continental margin, Strait of Juan de Fuca to Cape Mendocino. Technical report, US Geological Survey, 1993. doi: 10.3133/i2091A.

Gerya, T. V. and Meilick, F. Geodynamic regimes of subduction under an active margin: effects of rheological weakening by fluids and melts. *Journal of Metamorphic Geology*, 29(1):7–31, 2011. doi: 10.1111/j.1525-1314.2010.00904.x.

Han, S., Carbotte, S. M., Canales, J. P., Nedimović, M. R., Carton, H., Gibson, J. C., and Horning, G. W. Seismic reflection imaging of the Juan de Fuca plate from ridge to trench: New constraints on the distribution of faulting and evolution of the crust prior to subduction. *Journal of Geophysical Research: Solid Earth*, 121 (3):1849–1872, Mar. 2016. doi: 10.1002/2015JB012416.

Hayes, G. P., Moore, G. L., Portner, D. E., Hearne, M., Flamme, H., Furtney, M., and Smoczyk, G. M. Slab2, a comprehensive subduction zone geometry model. *Science*, 362(6410):58–61, Oct. 2018. doi: 10.1126/science.aat4723.

Kincaid, C. Subduction dynamics: From the trench to the core-mantle boundary. *Reviews of Geophysics*, 33(S1):401–412, 1995. doi: 10.1029/95RG00437.

Laurencin, M., Graindorge, D., Klingelhoefer, F., Marcaillou, B., and Evain, M. Influence of increasing convergence obliquity and shallow slab geometry onto tectonic deformation and seismogenic behavior along the Northern Lesser Antilles zone. *Earth and Planetary Science Letters*, 492:59–72, 2018. doi: 10.1016/j.epsl.2018.03.048.

Magni, V., Allen, M. B., van Hunen, J., and Bouilhol, P. Continental underplating after slab break-off. *Earth and Planetary Science Letters*, 474:59–67, 2017. doi: 10.1016/j.epsl.2017.06.017.

Marjanović, M., Carbotte, S. M., Nedimović, M. R., and Canales, J. P. Gravity and seismic study of crustal structure along the Juan de Fuca Ridge axis and across pseudofaults on the ridge flanks. *Geochemistry, Geophysics, Geosystems*, 12(5), 2011. doi: 10.1029/2010GC003439.

McCrory, P. A., Blair, J. L., Waldhauser, F., and Oppenheimer, D. H. Juan de Fuca slab geometry and its relation to Wadati-Benioff zone seismicity: JDF SLAB GEOMETRY AND WBZ SEISMICITY. *Journal of Geophysical Research: Solid Earth*, 117(B9), Sept. 2012. doi: 10.1029/2012JB009407.

Nolan, S., Trehu, A. M., Hooft, E. E., Ashraf, A., Wirth, E., Ward, K. M., and Stone, I. Cascadia 2021: Developing a 3-D Seismic Velocity Model Across the Central Cascadia Subduction Margin. In *AGU Fall Meeting Abstracts*, volume 2022, pages T32E–0189, 2022.

Parsons, T., Trehu, A. M., Luetgert, J. H., Miller, K., Kilbride, F., Wells, R. E., Fisher, M. A., Flueh, E., ten Brink, U. S., and Christensen, N. I. A new view into the Cascadia subduction zone and volcanic arc: Implications for earthquake hazards along the Washington margin. *Geology*, 26(3):199–202, 1998. doi: 10.1130/0091-7613(1998)026<0199:ANVITC>2.3.CO;2.

Schellart, W. P. and Rawlinson, N. Convergent plate margin dynamics: New perspectives from structural geology, geophysics and geodynamic modelling. *Tectonophysics*, 483(1-2):4–19, 2010. doi: 10.1016/j.tecto.2009.08.030.

Shuck, B., Gulick, S. P., Carbotte, S. M., Miller, N. C., Watt, J. T., Patton, J. R., Trehu, A. M., Greiner, K., Hagemeier, D., Briggs, R. W., et al. Filling in the Gap: Reprocessing Legacy Active-Source Seismic Data from the Southern Cascadia Subduction Zone to Assess Hazards. *American Geophysical Union, Annual Fall Meeting*, 2024.

Toomey, D. R., Allen, R. M., Barclay, A. H., Bell, S. W., Bromirski, P. D., Carlson, R. L., Chen, X., Collins, J. A., Dziak, R. P., Evers, B., et al. The Cascadia Initiative: A sea change in seismological studies of subduction zones. *Oceanography*, 27(2):138–150, 2014. doi: 10.1029/92JB00069.

Wang, K. and Tréhu, A. M. Invited review paper: Some outstanding issues in the study of great megathrust earthquakes—The Cascadia example. *Journal of Geodynamics*, 98:1–18, 2016. doi: 10.1016/j.jog.2016.03.010.

Yepes, H., Audin, L., Alvarado, A., Beauval, C., Aguilar, J., Font, Y., and Cotton, F. A new view for the geodynamics of Ecuador: Implication in seismogenic source definition and seismic hazard assessment. *Tectonics*, 35(5):1249–1279, 2016. doi: 10.1002/2015TC003941.

The article *Shoreline crossing Moho geometry of the Cascadia slab: CascadiaMoho1.0* © 2026 by Asif Ashraf is licensed under CC BY 4.0.